Nuclear Instruments and Methods in Physics Research B 266 (2008) 4959–4968

Contents lists available at ScienceDirect

Nuclear Instruments and Methods in Physics Research B

journal homepage: www.elsevier.com/locate/nimb

Secondary ion emission from Cu(100) surfaces with atomic adsorbates (N, O, Cl, S and Br)

M.A. Karolewski [a,*], R.G. Cavell [b]

[a] Department of Chemistry, University of Brunei Darussalam, Jalan Tungku Link, Gadong BE 1410, Brunei Darussalam
[b] Department of Chemistry, University of Alberta, Edmonton, AB, Canada T6G 2G2

ARTICLE INFO

Article history:
Received 13 June 2008
Received in revised form 16 August 2008
Available online 2 September 2008

PACS:
68.49.Sf
79.60.Dp
82.80.Ms

Keywords:
Secondary ions
Sputtering
Copper
Adsorption
Clusters

ABSTRACT

Several targets that consist of atomic species X (X = N, O, Cl, S, Br) adsorbed at hollow sites on the Cu(100) surface have been examined with low-fluence secondary ion mass spectrometry (SIMS). The positive and negative secondary ion (SI) abundance distributions, which show a range of characteristics, have been discussed with the aid of thermochemical data derived from ab initio calculations. In positive SIMS, CuX^+ is never observed, while the only heteronuclear (mixed-atom) SI that is observed for all five systems is Cu_2X^+. In negative SIMS, the dominant heteronuclear species for all systems is CuX_2^-, except for N/Cu(100), which produces no CuN_k^-, ions. Cu^- emission is observed only for O/Cu(100). By analogy with results from laser ablation studies of O/Cu targets, it is conjectured that Cu^- is a daughter product of the gas-phase dissociation of polyatomic Cu–O anion clusters.

1. Introduction

The explanation and prediction of secondary ion (SI) abundance distributions is a long-standing problem that remains one of the fundamental theoretical challenges of secondary ion mass spectrometry (SIMS). Even simple targets give rise to complex SIMS spectra due to the emission of SIs that can have a range of molecular formulae. For example, a target consisting of an atomic species X adsorbed on the surface of a metal M produces cluster ions of the form $M_jX_k^{\pm}$.

There have been many attempts to establish the information content of SI abundance distributions, especially their relationship to the surface structure and composition of the target [1]. SIMS spectra for molecular solids can be rationalised using fragmentation models analogous to those used for electron impact mass spectra [2]. For crystalline solids, the most extensive experimental data have been collected for oxidised metal surfaces and bulk metal oxides [3–6], but other classes of binary inorganic compounds including sulphides [7], halides [8,9] and borides [10] have also been surveyed.

SI abundance distributions differ sufficiently with composition for crystalline targets that they can be used for speciation purposes [1,11]. The statistical properties of cluster ion series such as $MO_k^{\pm}$ from metal (M) oxide targets can be described by a normal distribution depending on the index k [3]. It has been suggested that cluster ion yields reflect variations in the valence electron number (shell structure) of the corresponding cluster ions, and can thus provide information about the bonding state of the metal atom in the oxide [12]. In another approach, structural motifs in the target have been inferred from the structures of prominent cluster ions. For example, the Ni_2^+/Ni^+ yield ratio has been used as an indicator of the structural integrity of Ni crystal surfaces [13], while M_jCO^+/M_j^+ ratios have been used to characterise the bonding configurations of CO adsorbed on metal surfaces [14]. Correlations between target and SI structures have also been identified for SIMS data obtained from compound crystals [15].

This paper compares the characteristics of SIMS spectra measured for targets that consist of an atomic species X (X = N, O, Cl, S, Br) adsorbed on a Cu(100) single crystal surface (the SIMS data for S/Cu(100) have been presented previously [16]). To aid in the discussion of the experimental data, ab initio calculations of the thermochemical properties of a range of Cu_jX_k clusters and their ions have also been carried out.

* Corresponding author.
E-mail address: karolewski@alum.mit.edu (M.A. Karolewski).

0168-583X/$ - see front matter © 2008 Elsevier B.V. All rights reserved.
doi:10.1016/j.nimb.2008.08.009

The intention of this study was to examine the dependence of SI abundance distributions on the chemical properties of the adsorbate, while avoiding as far as possible the potentially confounding effects of structural differences. This approach is similar to that of Allen et al. who examined spinels with a range of metal atom compositions in order to separate the effects of composition changes from those of crystal structure [4]. The use of low-fluence bombardment conditions and single crystal substrates in this study ensures that the target surfaces remain structurally well-defined during the SIMS analysis. For X = N, Cl, S and Br, the high coverage adsorbate structures involve hollow site occupation, with 4-fold coordination of the adsorbate by (relaxed) surface Cu atoms [17–20]. In contrast, O/Cu(100) is a reconstructed surface and the adsorbate has only 3-fold coordination to surface, Cu atoms at the adsorption (hollow) site [21]. For X = O, Cl and Br, adsorbate coverages of about 0.5 ML can be achieved. The N/Cu(100) structure also has a theoretical maximum coverage of 0.5 ML. However, the maximum N coverage achievable via N_2^+ bombardment (Section 2) has not been established, and may be below 0.5 ML. S forms a (2×2) structure on Cu(100) that permits a maximum adsorbate coverage of only 0.25 ML. In summary, the structural environments for different adsorbates are not identical, but the similarities of structure extend to the following details: the adsorbate is located at surface hollow sites with similar primary coordination by 4 Cu atoms for all systems except O/Cu(100) (reconstructed hollow site, with 3-fold coordination), while the adsorbate surface coverages vary between 0.25 and 0.5 ML.

Early studies of cluster ion emission behaviour such as [3,5] were hampered by a lack of thermochemical data relating to clusters (which persists to this day). However, ab initio calculations of the quantities of interest have become more feasible in recent years. In this study, ab initio thermochemical properties are found to have some predictive or explanatory power for the positive cluster ion abundance distributions. Negative cluster ion abundance distributions correlate less consistently with SI thermochemical properties, and may instead reflect the abundance distributions of daughter products derived from anion dissociation processes.

2. Experimental

2.1. SIMS measurements

The Cu(100) specimen (in the form of a 1 cm diameter disc) was oriented by Laue diffraction to within 1° and then polished (1 μm diamond paste), chemically etched (HNO_3) and rinsed (water, 2-propanol) prior to insertion in the SIMS spectrometer, whose base pressure after bakeout was 10^{-10} mbar. The subsequent cleaning of the crystal in UHV involved numerous cycles of Ar^+ bombardment and heating (~1000 K), which reduced all contaminants to satisfactory levels, as determined by SIMS (e.g. for 1 nA Ar^+: C_2^-, CN^-, $Cl^- < 50$ counts s^{-1}; O^-, $C_2H^- < 10$ counts s^{-1}). Secondary ions were detected in the normal emission direction (using a 1–400 amu VG SXP400 quadrupole mass spectrometer). The angle between the primary beam direction and secondary ion emission direction was 45°. SIMS data were acquired using a rastered, micro-focussed ion source (VG AG61) with primary ion (4 or 5 keV Ar^+) current densities of 4–7 nA cm^{-2}, depending on sample SI yields. The target sample bias was adjusted to optimise the yields of cluster ion species. Overlayers of O, Cl, S and Br were prepared by exposing clean Cu(100) to reactive gases at ~320 K, which were dosed at low pressures via a leak valve. Ion-induced secondary electron current variations [22] were used to judge the saturation exposures (O_2: 200 L; Cl_2, H_2S, Br_2: 10 L), where 1 L = 10^{-6} torr s. The N overlayer was prepared by bombardment of Cu(100) with 3 keV N_2^+ ions (10 μA cm^{-2}, 300 s), followed by annealing at ~500 K.

2.2. Ab initio calculations

Ab initio calculations of cluster properties were carried out for neutral and ionic forms of CuX, Cu_2X, Cu_3X, and CuX_2 species (where X = N, O, Cl, S, Br or Cu) by means of density functional theory (DFT) using the Gaussian-03 suite of programs (revision B.05) [23]. The hybrid B3LYP exchange-correlation functional was used for the DFT calculations [24,25]. Scalar (spin-independent) relativistic effects were taken into account by employing the second-order Douglas–Kroll–Hess (DKH2) Hamiltonian [26]. For all clusters (i.e. neutrals and ions), except the C_{3v} Cu_3X^+ species, the structure optimisations and total energy calculations were carried out using the (all-electron) 6-311+G(3df) triple-zeta basis set, which is available for elements up to Kr and is supplemented by polarization and diffuse functions. Structure optimisations for the C_{3v} Cu_3X^+ species were performed using the smaller 6-31+G(3df) basis set, with a non-relativistic Hamiltonian (in order to circumvent convergence problems). Single-point energy calculations were then carried out at the optimised structure by the method employed for the other clusters.

For both Cu_2X and CuX_2 clusters, calculations were carried out for linear (D_{2h}) and bent (C_{2v}) geometries, and for CuX_2 clusters only, the bent $Cu(X_2)$ (C_s) geometry. For Cu_3X clusters, calculations were carried out for D_{3h} and C_{3v} geometries. For Cu_j clusters, an analogous range of structures was considered, as well as the optimum structures identified by prior theoretical studies. For all atoms and clusters, the DFT calculations were carried out for the electronic states having the lowest spin multiplicities; states of higher multiplicity were also examined for a few well-established exceptions (^4N, ^3O, ^3S, $^3O_2$, $^3S_2$) and for CuX, Cu_2X, Cu_3X, CuX_2 neutrals and ions with X = N, O and S. The DFT calculations form the basis of a database of total energies for neutral and ionized clusters, that includes about 250 distinct structures or electronic states, and is used to predict the molecular properties described below for the most stable neutral and ionic cluster species.

For each optimised neutral cluster structure the properties calculated were: binding (or atomization) energies (BE), vertical ionization potentials (IP), and vertical electron affinities (EA). Where required for computations of ion dissociation energies (see below) adiabatic IPs and/or EAs were also calculated after optimisation of cluster ion structures. The calculations neglect zero point energy corrections, which contribute less than 0.05 eV to relative energies. Results are reported only for the most stable geometry of each molecular formula. During a vertical transition the structure of the cluster does not change, but for clusters containing N, O or S atoms, the spin multiplicity may increase or decrease (the final state multiplicity that yields the smallest IP or largest EA is chosen).

Dissociation energies (D_+, D_-) for Cu_jX^+ and CuX_k^- cluster ions are estimated from the DFT results by consideration of the energetics of all possible dissociation processes that involve loss of a monatomic species (atom or ion) from the parent ion (the most facile process being chosen). For example, 6 such dissociation processes are possible for Cu_3X^+. The estimates of D_+ and D_- are based on the energies of the optimised ground state structures of each species (neutrals, ions) that appears in the dissociation scheme. The most facile $Cu_jX_k^\pm$ dissociation processes are found to be as follows: $CuX^+ \rightarrow Cu^+ + X$; $Cu_2X^+ \rightarrow Cu^+ + CuX$; $Cu_3X^+ \rightarrow Cu + Cu_2X^+$ (except $Cu_3N^+ \rightarrow Cu_3^+ + N$); $CuX^- \rightarrow Cu + X^-$ (except $CuN^- \rightarrow Cu^- + X$); $CuX_2^- \rightarrow CuX + X^-$ (except $CuO_2^- \rightarrow Cu^- + O_2$).

3. Results

3.1. Secondary ion mass spectra

Figs. 1–5 show positive and negative SIMS spectra measured for N, O, Cl, S and Br adsorbed on Cu(100). All adsorbates (X) produced a marked increase of both positive and negative SI emission relative to clean Cu(100). A clean Cu(100) surface gives rise to a $^{63}Cu^+$ yield of 30–50 counts per second for 1 nA incident Ar^+ (cps nA^{-1}). After adsorption of halogens, the $^{63}Cu^+$ intensity rises to 1.3×10^4 cps nA^{-1} for Cl, and 6×10^3 cps nA^{-1} for Br, whereas adsorption of N, O or S gives $^{63}Cu^+$ yields of about 100 cps nA^{-1}. In negative SIMS: the X^- yields associated with Cl (3×10^4 cps nA^{-1}) and Br adsorption (7×10^3 cps nA^{-1}) were much greater than those for O (130 cps nA^{-1}) and S (30 cps nA^{-1}) adsorption.

SIs produced by the X/Cu(100) targets can be categorised as elemental ions (e.g. Cu^+, O^-), homonuclear cluster ions (e.g. O_2^-, Cu_3^+) and heteronuclear (mixed-atom) cluster ions (e.g. Cu_2Cl^+, $CuCl_2^-$), respectively. The distinction between homo- and heteronuclear cluster ions is useful because the addition of a heteroatom leads to a large modification of cluster ion energetics.

Table 1 summarises the SI species that are dominant in, and absent from, the cluster ion series Cu_jX^+ and CuX_k^- observed for the various adsorption systems. The decline of quadrupole sensitivity with mass (roughly scaling as M^{-1} [27]) is not sufficiently rapid to overshadow the gross SI yield trends, because the major lines in question are separated by <100 amu. However, it should be appreciated that the spectra shown in Figs. 1–5 are generally less sensitive at the higher masses, so that the relative yields of larger clusters are underestimated. The absence of an ion in the experimental data implies that its yield is small relative to the most abundant ions (<0.1–1%, depending on the system), but not that its yield is zero.

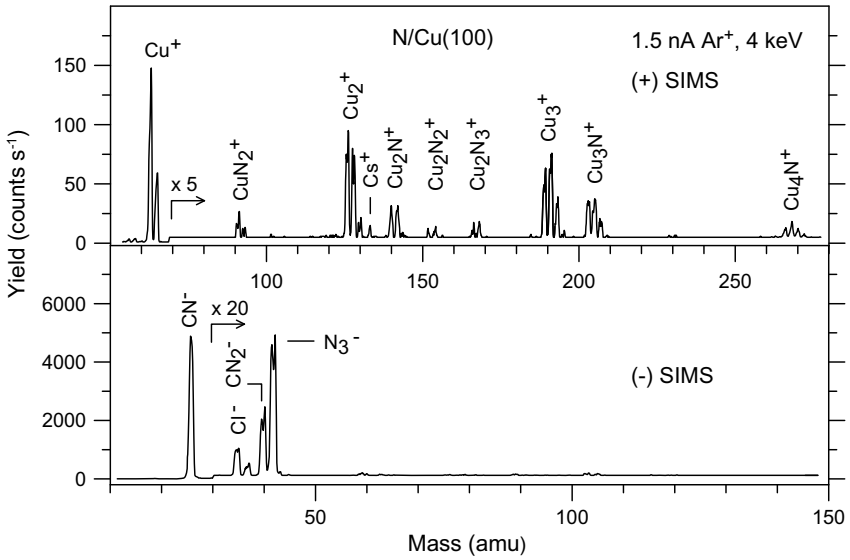

Fig. 1. Positive and negative secondary ion mass spectra for a N/Cu(100) target.

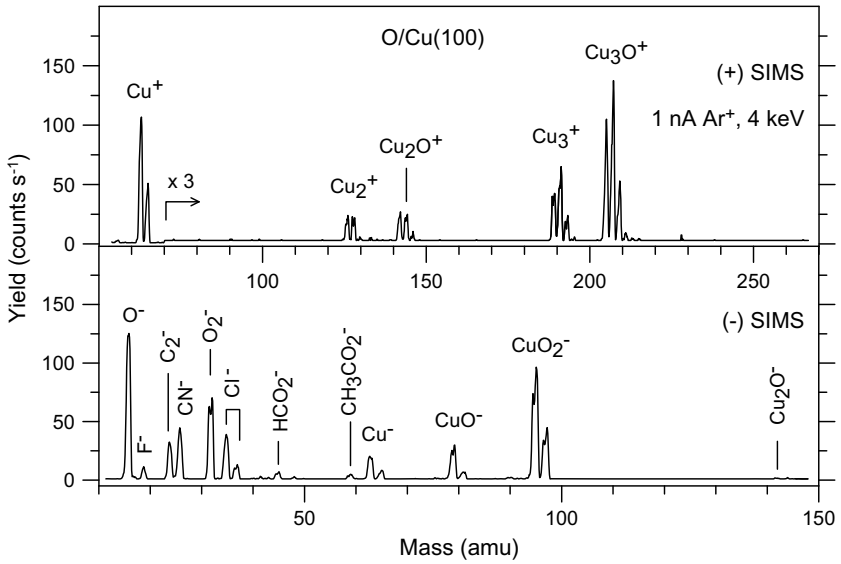

Fig. 2. Positive and negative secondary ion mass spectra for a O/Cu(100) target.

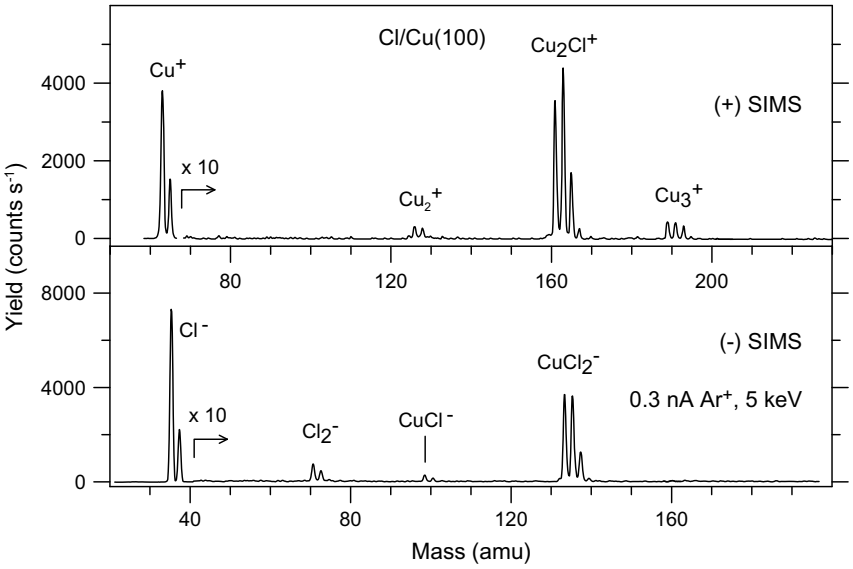

Fig. 3. Positive and negative secondary ion mass spectra for a Cl/Cu(100) target.

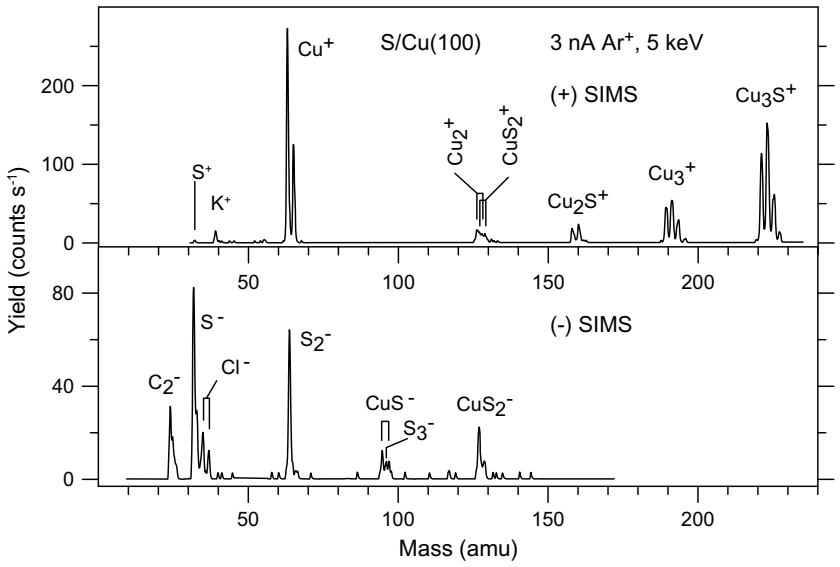

Fig. 4. Positive and negative secondary ion mass spectra for a S/Cu(100) target.

3.2. Positive SIMS

In positive SIMS, the most abundant clusters take the general form Cu_jX^+. However, the CuX^+ species ($j = 1$) are not observed for any system. For the halogen adsorbates (X = Cl, Br), only Cu_2X^+ is observed in the Cu_jX^+ series, whereas for X = N, O, S, both Cu_2X^+ and Cu_3X^+ are observed. For the N, O, S adsorbates, Cu_4X^+ emission can be detected at trace levels, but remains below detection limits for halogen adsorbates. Other Cu–X positive ion clusters that are observed for specific systems include CuX_2^+ (X = Br, S) and $Cu_2X_2^+$, $Cu_2X_3^+$ (X = N).

Cu^+, Cu_2^+ and Cu_3^+ emission are readily observed for all systems. The $Cu_3^+ : Cu_2^+$ ratio (corrected for isotopic distributions) varies in the relatively narrow range 1–3 for each system. A similar value for this ratio is reported for clean Cu [28]. The next member of this series, Cu_4^+, has a much lower yield than Cu_2^+ and Cu_3^+ and is difficult to observe under typical quadrupole operating conditions.

The yields of X^+ species are at least two orders of magnitude lower than the yields of Cu^+ and they are difficult to detect, or not detected, under low-fluence experimental conditions.

3.3. Negative SIMS

All systems, with the exception of N/Cu(100), produce clusters of the form CuX_k^- ($k = 1$ or 2). No CuX_3^- clusters were detected. For O, Cl, S and Br, the dominant cluster of the CuX_k^- type is CuX_2^-. For the halogen adsorbates (Cl, Br) CuX^- is either much weaker than CuX_2^- (Cl) or below detection limits (Br). However, for the chalcogen adsorbates (O, S), the CuX^- yield is comparable to that of CuX_2^-.

One or more elemental clusters of the form X_n^- was detected for all systems. The halogen adsorbates produce high yields of X^-, while X_2^- emission is much weaker (the Br_2^- yield is at the detection limit). For the chalcogen adsorbates, X^- and X_2^- have comparable

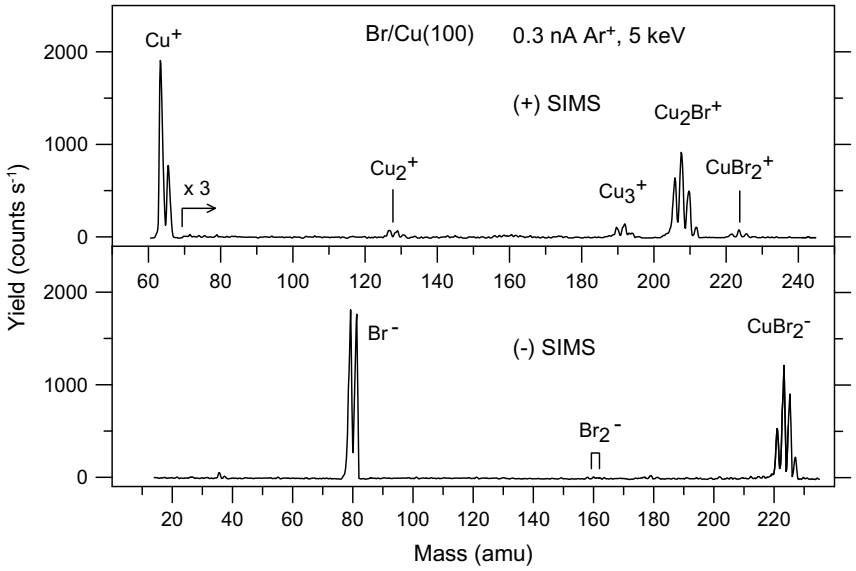

Fig. 5. Positive and negative secondary ion mass spectra for a Br/Cu(100) target.

Table 1
Dominant and absent secondary ion species observed in the series Cu_jX^+ and CuX_k^- for X/Cu(100) adsorption systems (where X represents Cl, Br, O, S or N)

	Positive SIMS		Negative SIMS	
	Dominant	Absent	Dominant	Absent
X = Cl and Br	Cu_2X^+	CuX^+, Cu_3X^+	CuX_2^-	CuX^-,[a] CuX_3^-
X = O and S	Cu_3X^+	CuX^+	CuX_2^-	CuX_3^-
X = N	Cu_2X^+, Cu_3X^+	CuX^+	–	CuX^-, CuX_2^-, CuX_3^-

[a] A low yield of $CuCl^-$ is observable for Cl/Cu(100).

yields. X_3^- emission is also readily observed for S/Cu(100). A unique feature of the O/Cu(100) system is the emission of Cu^-.

The negative SIMS spectrum of N/Cu(100) is distinct from those of the other systems. No CuN_k^- SIs are observed. The spectrum is dominated by N_3^- emission and various lines associated with surface impurities. In particular, intense emission of CN^- is observed that probably originates from a surface CN species. This contaminant may arise from a reaction between residual surface carbon and the N_2^+ ions used for the surface preparation. It is difficult to estimate the level of carbon contamination. No SI containing carbon (e.g. CuC^+, $CuCN^+$) can be detected in positive SIMS, but this result is inconclusive, since it was observed in this study that no CuC_k^+ cluster ions could be detected even after lengthy bombardment of Cu(100) with CH_4^+. A better gauge of surface contamination by carbon is the relative intensity of C_2^-, which is negligible in Fig. 1.

3.4. Cluster ion energetics

Tables 2–5 summarise the electronic states, binding energies (BE), ionization potentials (IP), electron affinities (EA) and threshold ion dissociation energies (D_+, D_-; see Section 2.2) that are predicted from DFT calculations for a range of clusters that are relevant to this study. Clusters $Cu_jX_k^{\pm}$ that contain X atoms from the same periodic group (i.e. O and S, or Cl and Br) are predicted to have closely similar structural and thermochemical properties. Experimental or theoretical estimates of BEs, IPs, EAs and ion dissociation energies are also shown in the tables (where available).

Resonant electron transfer processes involve vertical electronic transitions, and thus the vertical ab initio IPs and EAs listed in Tables 2–5 are the quantities relevant for use with the associated theoretical models (e.g. Eqs. (1) and (2) in Section 4.1). The thermochemistry of ion dissociation processes is better described using adiabatic IPs and EAs, which are also provided in the tables when required for computation of D_+ and/or D_-. Most experimental values of the IP and EA are adiabatic values. Vertical IPs (EAs) are numerically larger (smaller) than the adiabatic values, but are typically similar within 0.2 eV. However, considerable differences may arise if a molecular point group change takes place upon ionization. Such exceptional cases are indicated in footnotes in Tables 2–5. Only a limited survey of possible cluster (and ion) structures has been carried out in this study. An incorrect structural assignment represents a potential source of quantitative error in the tables, especially for the Cu_3X^+ clusters that have a large range of possible structures, and have not been previously studied either experimentally or theoretically.

Some of the data in Tables 2–5 will be required for the discussion relating to ionization mechanisms in Section 4. The EA (IP) data for clusters that are only observed as positive (negative) ions serves primarily to test the accuracy of the ab initio method, and will not be used for the discussion. The BE and adiabatic IP or EA data given in Tables 2–5 can be used to reconstruct the tabulated values of D_+ and D_- to within ±0.1 eV; e.g. for the process $CuX^- \rightarrow Cu + X^-$, $D_- = BE(CuX) + EA(CuX) - EA(X)$.

The accuracy of DFT predictions based on the B3LYP method for a range of small CuM molecules (M represents an atomic or molecular fragment) has been reviewed in [29]. Mean errors below 0.5 eV may be expected in the property values (BE, IP, EA, D_+ and D_-) presented in Tables 2–5. A comparison between the ab initio predictions and the available literature estimates in Tables 2–5 generally bears this out, except for the EA of CuN^-. Based on the failure to observe photoemission from CuN^- from a mixture of laser-ablated Cu clusters and NO, it was argued in [54] that the EA of CuN^- was above the photon energy of 3.3 eV. However, this estimate is improbably high: the only diatomic molecule known to have an EA > 3.3 eV is CN [51].

Ab initio data are not reported for CuX_3 clusters in this work, because no cluster of this type was observed in the experimental SIMS data, and because calculations for these clusters were found to be prone to convergence problems. A range of isomeric forms with distinct thermochemical properties can be expected. For example, the isomers of CuO_3 have been examined in detail in

Table 2
DFT predictions of binding energies (BE), vertical ionization potentials (IP) and electron affinities (EA) and threshold ion dissociation energies (D_+, D_-) for CuX clusters and Cu

	BE (eV)	IP (eV)	EA (eV)	D_+ (eV)	D_- (eV)	References
Cu (^{2}S)	–	8.3 7.7	1.3 1.2	–	–	[51,52]
CuN ($^3\Sigma$)	2.0 (1.2*)	9.2 [9.2] [a] 7.9*	1.0 [1.0][a] >3.3	1.1 0.3*, 0.8*	1.8	[53–55]
CuO [$^2\Pi$]	2.9 (2.8)	9.5 [9.5][b] 9.9, 9.4, 9.2*	1.6 [1.6] 1.8	1.6 1.4, 0.6–1.3*	2.9 (3.1)	[51,53,56–61]
CuCl ($^1\Sigma$)	3.5 (3.9)	10.1 [10.1] 10.7	1.4 [1.5]	1.7	1.3	[62]
CuS [$^2\Pi$]	2.8 (2.8)	8.7 [8.7][b] 8.7*, 9.9*	2.1 [2.1] 1.9–2.0*	2.3 2.1	2.7 (2.6)	[60,63–66]
CuBr ($^1\Sigma$)	3.2 (3.5)	9.7 [9.7]	1.4 [1.5]	1.8	1.2	[63]
Cu_2 ($^1\Sigma_g$)	1.9 (1.8–2.0)	8.3 [8.2] 7.9	0.9 [0.9] 0.8	2.0 1.6	1.6	[51,62,67–70]

Electronic states are indicated by parentheses (this study) or square braces (previous studies); X designates states of undetermined symmetry. Upper lines of each row: DFT predictions; lower lines: experimental and theoretical (*) literature values. Some adiabatic IPs/EAs are given in square braces.
[a] Predicted symmetries of CuN^+ and CuN^- are $^4\Sigma$.
[b] Predicted symmetries of CuO^+ and CuS^+ are $^3\Sigma$.

Table 3
DFT predictions of binding energies (BE), ionization potentials (IP) and electron affinities (EA) for clusters of molecular formula Cu_2X (X = N, O, Cl, S, Br or Cu). The predicted Cu_2X^+ threshold ion dissociation energies (D_+) are also shown

	BE (eV)	IP (eV)	EA (eV)	D_+ (eV)	References
Cu_2N ($^2B_1$)	4.3	8.1 [8.1][a]	1.2 1.1	2.5	[54]
Cu_2O ($^1A_1$)	5.6 6.7	8.1 [7.8] 7.8*,[b]	1.2 1.1	3.2	[71,72]
Cu_2Cl ($^2A_1$)	4.6	7.2 [6.8]	1.5	2.5	
Cu_2S ($^1A_1$)	5.6 6.2*	7.9 [7.8] 6.7*,[b]	1.2	3.2	[71,73]
Cu_2Br ($^2A_1$)	4.2	7.1 [6.8]	1.5	2.5	
Cu_3 ($^2A_1$)	2.9 2.9	6.1 [6.0][c] 5.8	1.0 [2.2][d] 2.3	3.2 2.7–2.8	[51,67,68,70]

All clusters have C_{2v} symmetry, except as noted. See the footnote of Table 2 for further information.
[a] Lowest electronic state of Cu_2N^+ is $^3A_2$.
[b] Prediction of vertical IP at Hartree–Fock level.
[c] Point group of Cu_3^+ is D_{3h}.
[d] Point group of Cu_3^- is $D_{\infty h}$.

Table 4
DFT predictions of binding energies (BE), ionization potentials (IP) and electron affinities (EA) for clusters of molecular formula Cu_3X (X = N, O, Cl, S, Br or Cu). The predicted Cu_3X^+ threshold ion dissociation energies (D_+) are also shown

	BE (eV)	IP (eV)	EA (eV)	D_+ (eV)	References
Cu_3N ($^1A_1$)	6.9	7.7 [6.2][a]	1.1	3.1	
Cu_3O ($^2A_1$)	7.2	6.5 [6.3]	1.3	3.1	
Cu_3Cl ($^1A_1$)	6.0	7.3 [7.1]	1.2	1.1	
Cu_3S ($^2A_1$)	7.0	6.3 [6.1]	1.4	3.2	
Cu_3Br ($^1A_1$)	5.7	7.2 [7.0]	1.3	1.2	
Cu_4 (^1A_g)	5.1 5.2 ± 0.6	6.9 [6.9] 7.0 ± 0.6	1.4 [1.5] 1.3	1.4 0.7–1.1	[51,62,67,68]

All clusters have C_{3v} symmetry, except Cu_4 (D_{2h}) and as noted. See the footnote of Table 2 for further information.
[a] Point group of Cu_3N^+ is D_{3h}.

[30,31]. Three CuO_3 isomers are found within a BE range of 0.24 eV; all isomers have similar IPs (within 10%), but one isomer has a lower EA (1.0 eV) than the other two (~2.5 eV).

4. Discussion

4.1. Ionization mechanisms

The goal of this discussion will be to identify the molecular and target properties that determine the cluster SI abundance distributions, through comparisons between the experimental observations and candidate properties of the target (structure, composition and work function) and the clusters (IP, EA, D_+ and D_-). To some extent, the measurements reported in this study control for the effects of target structure and composition, except as noted in Section 1. However, target structure does not appear to exert a strong influence on SI abundance distributions. For exam-

Table 5
DFT predictions of binding energies (BE), ionization potentials (IP) and electron affinities (EA) for clusters of molecular formula CuX_2 (X = N, O, Cl, S or Br). The predicted CuX_2^- threshold ion dissociation energies (D_-) are also shown

	BE (eV)	IP (eV)	EA (eV)	D_- (eV)	References
CuN_2[a] (^2X)	1.5	11.7	3.4 [3.5]	−6.3	
CuO_2[b] ($^2A''$)	6.0 5.8*	9.6	0.9 [2.1][c] 1.5	1.4	[51,74]
$CuCl_2$[a] [$^2\Pi_g$]	6.1 6.4, 6.7*	11.8 12.0	4.1 [4.1] 4.4	3.1	[75–77]
CuS_2[b] ($^2A''$)	5.9	8.4	1.7 [2.0][c]	1.8	
$CuBr_2$[a] (^2X)	5.4	10.9	4.1 [4.1] 4.4	2.8	77

See the footnote of Table 2 for further information.
[a] Linear molecule ($D_{\infty h}$).
[b] Molecule has C_s symmetry, corresponding to $Cu(X_2)$ adduct.
[c] Anions have $D_{\infty h}$ symmetry, corresponding to $(XCuX)^-$ structure.

ple, SIMS and even laser ablation mass spectra from bulk Cu halide [32–34] and sulphide [7] targets display heteronuclear SI abundance distributions that do not differ qualitatively from those produced by the corresponding adsorbate systems. The discussion in Sections 4.2 and 4.3 will be restricted to a consideration of relative SI yields (abundance distributions) on the assumption that their behaviour is largely independent of the (incompletely understood) global SI yield enhancements due to work function shifts and other causes, which are now briefly considered.

Two broad classes of proposed mechanisms for SI emission from metallic surfaces can be distinguished: those in which (1) ionization involves electron transfer between the target and a departing sputtered particle (electron transfer models, such as the tunnelling or surface excitation models), or (2) ionization is a consequence of, or results in, heterolytic dissociation of clusters (cluster dissociation models). The various models have been described in a number of reviews, e.g. [35–39].

Electron transfer models of SI emission typically predict an exponential dependence of the ion fraction on the target work function (φ), e.g. the Nørskov–Lundqvist model [40]:

$$Y^+/Y^0 \propto \exp\{-\alpha(IP-\phi)\} \quad (1)$$

$$Y^-/Y^0 \propto \exp\{-\alpha(\phi-EA)\} \quad (2)$$

where α is a parameter that depends on the target-SI combination and on SI kinematic properties, and $Y^{\pm}$ and Y^0, respectively, are the sputter yields of the ionic and neutral species. According to Eqs. (1) and (2), positive work function shifts ($\Delta\varphi > 0$) should always enhance positive SI yields, and attenuate negative SI yields. The X/Cu(100) adsorbate induced work function shifts are typically positive (except for N): N/Cu(100): −0.1 eV [41]; O/Cu(100): 0.1 eV [41]; Cl/Cu(100): 1.1 eV [42]; S/Cu(100): 0.3 eV [41]; Br/Cu(100): 0.9 eV [43]. The adsorbate-induced SI yield enhancements observed in this study are consistent with Eq. (1) (for positive ions, except for N/Cu(100)), but not with Eq. (2) (for negative ions). For example, the largest absolute yields of both positive and negative SIs are associated with the halogen adsorbates, which also induce the largest positive work function shifts. Difficulties in applying Eqs. (1) and (2) to SI yield enhancements produced by electronegative adsorbates have long been acknowledged [35,38,44], although good agreement with Eq. (2) in negative SIMS is reported for alkali metal adsorbates [38].

Theoretical relationships of the form of Eqs. (1) and (2) connect SI yields to the ionization energetics of sputtered particles. If the relationships were valid, individual SI yields would correlate with IPs in positive SIMS, or with EAs in negative SIMS. However, in cluster dissociation models, SI abundance distributions are determined by the survival probabilities (i.e. stabilities) and daughter products of sputtered species. An objective measure of the stability of a cluster ion is its dissociation energy.

The lack of knowledge concerning the quantum states of neutral and ionized clusters during sputtering complicates the discussion of ion formation energetics. In this study, ground state properties inferred from the (not comprehensive) DFT calculations will be assumed, but this approach is clearly open to question since ionization may involve excited electronic states. The different energetic properties of the two ion formation mechanisms (electron transfer versus cluster dissociation) provide a possible basis for discrimination between the mechanisms. However, cluster ion dissociation energies do depend on cluster IPs to some extent. Fig. 6 depicts a thermochemical cycle which shows that the cluster IP is a leading term in the computation of the dissociation energy (D_+) for any positive cluster ion CuZ^+ that dissociates by loss of a Cu neutral (Z is any fragment). An increase in the CuZ IP (other things being equal) will tend to reduce the ion dissociation energy for CuZ^+ and vice versa. A similar relationship exists between the EA of CuZ and the ion dissociation energy for CuZ^-.

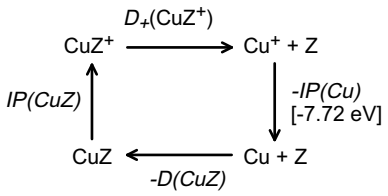

Fig. 6. A thermochemical cycle that connects dissociation energies for CuZ neutral and positive ion clusters respectively, where Z is any polyatomic fragment (IP: ionization potential and D, D_+: dissociation energies for neutral and positive ion clusters).

4.2. Homonuclear cluster ions

The abundance distributions of Cu_j^+ cluster ions from X/Cu(100) targets have the characteristic that Cu_2^+ and Cu_3^+ are the major SIs of this type (with yields for Cu_3^+ > yields for Cu_2^+), while Cu_4^+ yields are near, or below, the detection threshold. This behaviour resembles that reported for clean Cu targets [28,45,46]. This is understandable, since 50–75% of the atoms exposed at the X/Cu(100) target surfaces are atoms of the Cu lattice.

The Cu_j^+ abundance distributions (for Cu targets) have been explained in terms of electronic shell effects, whereby discontinuities in the abundance distributions are associated with IP extrema [47]. For example, Cu_3 is less abundant than Cu_2 in the flux of sputtered neutrals [28,45,46], whereas the yield of Cu_3^+ exceeds that of Cu_2^+. Thus, the preferential ionization of Cu_3, whose IP is 2 eV below that of Cu_2, must be sufficient to outweigh the lower sputter yield of Cu_3 species. The IP of Cu_4 is similar to that of Cu_3, so a similar line of reasoning would predict a relative decline of the yield of Cu_4^+ relative to Cu_3^+ (as observed) due to the lower sputter yield of Cu_4 neutrals. These arguments rely on the assumption that a lower IP will tend to increase the efficiency of ionization, but do not explain the mechanism involved.

Collision-induced fragmentation pathways of Cu_j^+ cluster ions have been studied in detail by Krückeberg et al. [67]. The experimental dissociation energies (D_+) for $j = 2$, 3, 4 were found to be 1.6, 2.8 and 1.1 eV, respectively (the DFT predictions in Tables 2–4 are similar). Thus, for sputtered Cu cluster ions that are formed in a range of excited states, Cu_3^+ is expected to be less susceptible than Cu_2^+ or Cu_4^+ to dissociation. In [67] it was also observed that Cu_4^+ dissociation produces Cu_3^+ and Cu, while Cu_3^+ dissociation produces Cu^+ and Cu_2. Thus, any dissociation of Cu_4^+ would also tend to increase the observed $Cu_3^+ : Cu_2^+$ ratio.

In summary, the preceding analyses demonstrate that the values of the IP and D_+ are such that ion formation mechanisms based on electron transfer and cluster dissociation, respectively, are both able to account qualitatively for the preferential production of Cu_3^+.

Table 6
Adiabatic electron affinities (EAs) for X, X_2 and X_3 species (X = N, O, Cl, S, Br and Cu)

X	EA (eV)		
	X	X_2	X_3
N	<0	<0	(2.7)
O	1.6 (1.5)	0.5 (0.5)	(2.1)
Cl	3.7 (3.6)	2.8 (2.4)	(5.1)
S	2.2 (2.1)	1.6 (1.7)	(2.1)
Br	3.5 (3.4)	2.9 (2.6)	(4.6)
Cu	1.3 (1.2)	0.9 (0.8)	(2.3)

Values outside parentheses are DFT predictions from this study. Experimental values [51,78] are given in parentheses.

Table 6 summarises experimental EA data for homonuclear clusters that are relevant for this study. The principal negative homonuclear cluster ion observed in the SIMS spectra is X_2^-. However, N_2^- is not observed, and Br_2^- is barely detectable. The absence of N_2^- or N^- emission is clearly due to the negative electron affinities of N_2 and N. Dissociation of both Cl_2^- and Br_2^- requires 1.2–1.3 eV [78] and the dimer EAs are also similar (Table 6), so the low yield of Br_2^- in contrast to Cl_2^- cannot be easily rationalised in energetic terms. The X_3^- ions of all adsorbate species are electronically stable (in the sense that EA > 0), but this type of ion is only observed in significant yield for X = N. The EAs of the trihalide species are higher than that for N_3, so again the energetics of electron attachment cannot account for the disparity of yields. A possible reason for the failure to observe X_3^- ions other than N_3^- in significant yields is dissociation of these ions prior to detection due to their production in excited states. For example, the energy required to dissociate Cl_3^- and Br_3^- via the reaction $X_3^- \rightarrow X + X_2^-$ is <1.3 eV [78].

4.3. Heteronuclear cluster ions

4.3.1. Positive cluster ions, Cu_jX^+

It has often been noted that the abundance distributions of secondary ions produced from ionic compounds reflect the operation of a simple electron shell-filling rule [48]. The results shown in Figs. 1–4 and in Table 1 indicate that similar patterns of positive cluster ion emission are observed for chemisorbed Cu(100) surfaces when the adsorbed atoms derive from the same periodic group. Three distinct patterns of emission can be associated with, respectively, the halogen (Cl and Br), chalcogen (O and S) and nitrogen adsorbates.

For all systems except N/Cu(100) the molecular formulae of the dominating positive SIs can be predicted on the basis of a shell-filling rule by assigning the conventional oxidation states of +1 to Cu, −1 to the halogens, and −2 to the chalcogens. The SI corresponding to the conventional −3 oxidation state of N, Cu_4N^+, is not the dominating species for N/Cu(100), but its yield is of the same order as the Cu_2N^+ and Cu_3N^+ species (the only system for which this happens). The shell-filling rule clearly works quite well for the systems other than N/Cu(100). The theoretical challenge is to identify what thermochemical property is responsible for the rule. As discussed in Section 4.1, two candidate properties are the IP and the ion dissociation energy (D_+).

DFT predictions of the IP and D_+ data that are relevant for the heteronuclear Cu_jX^+ SIs are collected in Tables 2–4. Trends in the Cu_jX^+ dissociation energies cannot be used in isolation to predict the dominant SIs. For example, D_+ values for Cu_2X^+ and Cu_3X^+ species are similar if X = O or S. However, it is noteworthy that all observable Cu_jX^+ species have $D_+ \geqslant 2.5$ eV, while those having $D_+ < 2.3$ eV (i.e. all CuX^+ species, Cu_3Cl^+ and Cu_3Br^+) are not observed. This apparent correspondence between D_+ values and SI observability may partly be fortuitous, since the DFT calculations are only expected to be accurate to ~0.5 eV (Section 3.4).

Various correlations between the IPs and relative yields of Cu_jX^+ SIs can also be identified. Between $j = 2$ and 3, the Cu_jX IPs fall by ~1.5 eV for X = O and S, by 0.9 eV for X = N, and remain invariant for X = Cl or Br. These IP properties correlate qualitatively with the observed variations in the Cu_3X^+/Cu_2X ratios: the ratios are on the order of 10 for X = O and S, near unity for X = N, and below detection limits (<1%) for X = Cl and Br. Between $j = 1$ and 2, the Cu_jX IPs also fall. For the chalcogen and halogen adsorbates, the IP of CuX is ~3 eV larger than that of Cu_2X, while the difference in IPs for CuN and Cu_2X is 1.1 eV. The relatively high IPs associated with CuX clusters again correlate with the observed absence of CuX^+ SIs.

Three conclusions concerning positive cluster SI emission emerge from these comparisons. (a) SIs with small ion dissociation energies are not observed. (b) The relative Cu_jX^+ yields from each target are largest for the SIs that have the lowest IPs (this implies that when Cu_3X^+ species dominate, the yield enhancement due to the lower IP must be sufficient to offset the yield disadvantage associated with the presumably lower clustering probability). (c) The mechanistic significance of the observed correlations between yields and molecular properties is not free of ambiguity: e.g. the absence of CuX^+ emission can be rationalised equally well in terms of the high IPs of CuX clusters, or the low dissociation energies of CuX^+ SIs.

4.3.2. Negative cluster ions, CuX_k^-

An electron shell-filling rule like that discussed for positive ions in the previous section would not anticipate the absence of CuN^-, which is a stable ion (unlike CuN_2^-), but could be used to rationalise the dominance of CuX_2^- species and low yields of CuX^- for the halogen systems (in CuX_2^- the valance of the halogen atoms is satisfied, while in CuX^- the halogen atom is hypervalent). The valence of chalcogen atoms can be satisfied by bonding of either atomic or diatomic units to Cu, which offers the possibility of producing either CuX^- or $Cu(X_2)^-$ closed-shell species. In this sense, there is no conflict between the shell-filling model and the behaviour of the chalcogen systems, even if the model has little predictive value.

The relative abundances of CuX_k^- anions observed in negative SIMS show some suggestive correlations with cluster EAs and cluster ion dissociation energies. For the halogen systems, the EA and D_- values for CuX_2^- species significantly exceed those for CuX^- species, whereas qualitatively opposite behaviour (but with less spread in the range of values) is found for the chalcogen systems (Tables 2 and 5). In principle, these trends in ion energetics are consistent with the experimental SIMS data, which show high (low or zero) yields of CuX_2^- (CuX^-) for the halogen systems, and comparable yields of both ion types for the chalcogen systems. However, ion energetics alone cannot necessarily explain why CuX_3^- species are not detected; CuX_3 species having adduct structures of the form $(CuX)X_2$ are expected to have large EAs comparable to those of X_2 molecules [30]. Likewise, the failure to observe CuN^- is not obviously due to ion energetics (the EA and D_- values of CuN^- are greater than those of the readily observed CuO_2^- species). Thus, it seems probable that other factors in the ion emission mechanism, such as ion chemistry or kinetics, may be responsible for the absence of these species in negative SIMS.

There is experimental evidence from laser ablation studies to suggest that some large secondary anions are not detected because of in-flight dissociation. The experimental SIMS spectrum reflects the abundance distribution of SI species at the detector. As others have pointed out, fragmentation of anion clusters produced in sputtering is probable on the general grounds that these processes take place at high effective temperatures, while excited states of anions are susceptible to dissociation via a range of mechanisms [36,38]. Since anion dissociation processes normally take place on a timescale shorter than the time of flight, daughter products will predominate at the detector, leading inevitably to a smaller mean cluster ion size than in the initial cluster ion population. This idea can be supported for O/Cu(100) system using data obtained from laser ablation experiments. Cu–O clusters can be produced by laser ablation of Cu in He/O_2 in a variety of isomeric forms [49,50]. Large CuO_k^- clusters (with $k > 2$) are susceptible to unimolecular photodissociation (at 3.5–4.7 eV), on a μs timescale, into Cu^- and either O_2 or O_3 (depending on the isomeric form of the cluster). The most abundant anion cluster produced by laser ablation is CuO_2^-. In negative SIMS, CuO_2^- is also the most abundant Cu–O anion. By analogy with the behaviour of laser-ablated clusters, the failure to observe CuO_3^- and larger CuO_k^- ions in negative SIMS, and the presence of Cu^- (a species unique to O/Cu(100)), may be

due to in-flight cluster dissociation. Experimental laser ablation studies show that for a photon energy on the order of 3 eV several distinct channels for both CuO_2^- and CuO_3^- photodissociation are available, leading to a variety of daughter products including neutral and anionic Cu, CuO, O_2 and O_3 [31,49,50]. The underlying reason for the emission of Cu^- is probably that the EA of Cu is greater than that of O_2 (Table 6), which will favour the production of Cu^- over O_2^- in any CuO_k^- dissociation process. For example, the ab initio predictions indicate that the dissociation of CuO_2^- into Cu^- and O_2 requires an excitation energy of 1.4 eV (Table 5), while other possible dissociation pathways require 2.2–3.6 eV. Ionic dissociation may prove to be the reason for the lack of emission of CuX_3^- SIs for other systems, but there is only limited experimental evidence to support this at present, e.g. Gronewald et al. observed fragmentation of $CuCl_3^-$ (but not $CuCl_2^-$) sputtered from $CuCl_2$ and CuCl salts [32].

5. Conclusions

Secondary ion mass spectra have been reported for targets that consist of atomic species (N, O, Cl, S, Br) adsorbed at hollow sites on Cu(100). The abundance distributions of secondary ion clusters show a range of characteristics that have been discussed with the aid of thermochemical data derived from ab initio calculations. The lack of knowledge concerning the quantum states of neutral and ionized clusters during sputtering considerably complicates the prediction and analysis of ion formation energetics.

The positive SIMS spectra of these systems become less complex as the electronegativity of the adsorbate X increases. For the most electronegative adsorbates there is greater adherence to electron shell-filling rules. Accordingly, the positive SIMS spectra for Cl/Cu(100) and Br/Cu(100) are dominated by the Cu_2X^+ line. In contrast, the positive SIMS spectrum of N/Cu(100) can be compared to that of a metallic alloy, for which all combinations of atoms occur. The SIMS spectra for O/Cu(100) and S/Cu(100) show behaviour that is intermediate between these limiting cases. The negative SIMS spectra for all systems consist of triatomic or smaller cluster ions. For the halogen systems, CuX_2^- emission predominates, while for the chalcogen systems, CuX^- emission is also significant. The negative SIMS spectrum of N/Cu(100) is devoid of cluster ions other than N_3^- and contaminants.

The only heteronuclear SI that is observed for all five systems is Cu_2X^+. It is particularly striking that the stable CuX^+ species are never observed. This indicates that cluster abundance distributions are not simply due to statistically determined recombination processes, but must satisfy other criteria that are presumed to be thermodynamic or kinetic in nature. The mechanistic significance of correlations between cluster ion yields and their thermochemical properties in positive SIMS is not free of ambiguity. The patterns of Cu_j^+ and Cu_jX^+ emission can be rationalised equally well in terms of trends in IPs, or ion dissociation energies (and, conceivably, other properties that have not been considered in this study). Consequently, it has been argued that SIMS data alone cannot normally be used to discriminate between electron transfer and cluster dissociation mechanisms of positive SI formation. The abundance distributions of negative SIs may include significant contributions from the fragmentation of anion clusters. It is conjectured that Cu^- emission from O/Cu(100) is a daughter product of the gas-phase dissociation of larger Cu–O clusters.

References

[1] L. van Vaeck, A. Adriaens, R. Gijbeis, Mass Spectrom. Rev. 18 (1999) 1.
[2] A.M. Spool, Surf. Interface Anal. 36 (2004) 264.
[3] C. Plog, L. Wiedmann, A. Benninghoven, Surf. Sci. 67 (1977) 565.
[4] G.C. Allen, J.M. Dyke, S.J. Harris, J. Chem. Soc., Faraday Trans. 87 (1991) 875.
[5] M.J. van Craen, F.C. Adams, Surf. Interface Anal. 5 (1983) 239.
[6] K.D. Klöppel, E. Jegers, G. von Bünau, Int. J. Mass Spectrom. Ion Processes 49 (1983) 11.
[7] G.J. Vandentop, M.A. Karolewski, R.G. Cavell, Int. J. Mass Spectrom. Ion Processes 89 (1989) 319.
[8] F. Honda, G.M. Lancaster, Y. Fukuda, J.W. Rabalais, J. Chem. Phys. 69 (1978) 4931.
[9] C. Plog, W. Gerhard, Surf. Sci. 152/153 (1985) 127.
[10] P. Wilhartitz, M. Grasserbauer, Mikrochim. Acta 89 (1986) 313.
[11] Z.P. Li, K. Hirokawa, Appl. Surf. Sci. 220 (2003) 136.
[12] W. Gerhard, C. Plog, Z. Phys. B 54 (1983) 59.
[13] R.S. Bordoli, J.C. Vickerman, J. Wolstenholme, Surf. Sci. 85 (1979) 244.
[14] A. Brown, J.C. Vickerman, Surf. Sci. 151 (1985) 319.
[15] R. Buhl, A. Preisinger, Surf. Sci. 47 (1975) 344.
[16] G.J. Vandentop, M.A. Karolewski, R.G. Cavell, Surf. Sci. 202 (1988) 457.
[17] H.C. Zeng, R.N.S. Sodhi, K.A.R. Mitchell, Surf. Sci. 188 (1977) 599.
[18] P.H. Citrin, D.R. Hamann, L.F. Mattheiss, J.E. Rowe, Phys. Rev. Lett. 49 (1982) 1712.
[19] H.C. Zeng, R.N.S. Sodhi, K.A.R. Mitchell, Surf. Sci. 177 (1986) 329.
[20] T.W. Fishlock, J.B. Pethica, R.G. Egdell, Surf. Sci. 445 (2000) L47.
[21] M. Kittel, M. Polcik, R. Terborg, J.-T. Hoeft, P. Baumgärtel, A.M. Bradshaw, R.L. Toomes, J.-H. Kang, D.P. Woodruff, M. Pascal, C.L.A. Lamont, E. Rotenberg, Surf. Sci. 470 (2001) 311.
[22] M.A. Karolewski, R.G. Cavell, Surf. Sci. 198 (1988) 118.
[23] Gaussian Inc., Pittsburgh PA.
[24] A.D. Becke, J. Chem. Phys. 98 (1993) 5648.
[25] C. Lee, W. Yang, R.G. Parr, Phys. Rev. B 37 (1988) 785.
[26] M. Barysz, A.J. Sadlej, Theochem 573 (2001) 181.
[27] F.G. Rüdenauer, Vacuum 22 (1972) 609.
[28] K. Franzreb, A. Wucher, H. Oechsner, Phys. Rev. B 18 (1991) 14396.
[29] A. Luna, M. Alcami, O. Mó, M. Yáñez, Chem. Phys. Lett. 320 (2000) 129.
[30] K. Deng, J. Yang, Q. Zhu, J. Chem. Phys. 113 (2000) 7867.
[31] Z. Cao, M. Solà, H. Xian, M. Duran, Q. Zhang, Int. J. Quantum Chem. 81 (2001) 162.
[32] G.S. Groenewold, A.D. Appelhans, G.L. Gresham, J.C. Ingram, A.D. Shaw, Int. J. Mass Spectrom. Ion Processes 178 (1998) 19.
[33] J. Lin, A.T.S. Wee, A.C.H. Huan, K.L. Tan, Surf. Sci. 285 (1993) 31.
[34] C.F. Ding, Y.Yu.H. Jensen, W.J. Balfour, C.X.W. Qian, Chem. Phys. Lett. 331 (2000) 163.
[35] G. Blaise, A. Nourtier, Surf. Sci. 90 (1979) 495.
[36] P. Williams, Surf. Sci. 90 (1979) 588.
[37] P. Williams, Appl. Surf. Sci. 13 (1982) 241.
[38] M.L. Yu, Nucl. Instr. Meth. B 15 (1986) 151.
[39] Z. Šroubek, J. Lörinčik, Surf. Rev. Lett. 6 (1999) 257.
[40] J.K. Nørskov, B.I. Lundqvist, Phys. Rev. B 19 (1979) 5661.
[41] G.G. Tibbetts, J.M. Burkstrand, J.C. Tracy, Phys. Rev. B 15 (1977) 3652.
[42] F. Jona, D. Westphal, A. Goldmann, P. Marcus, J. Phys. C 16 (1983) 3001.
[43] K. Kleinherbers, H.-G. Zimmer, A. Goldmann, Surf. Sci. 167 (1986) 417.
[44] P. Williams, C.A. Evans, Surf. Sci. 78 (1978) 324.
[45] I. Katakuse, T. Ichihara, Y. Fujita, T. Matsuo, T. Sakurai, H. Matsuda, Int. J. Mass. Spectrom. Ion Processes 67 (1985) 229.
[46] H. Gnaser, W.O. Hofer, Appl. Phys. A 48 (1989) 261.
[47] M. Knickelbein, Chem. Phys. Lett. 192 (1992) 129.
[48] G.S. Groenewold, A.D. Appelhans, G.L. Gresham, J.C. Ingram, A.D. Shaw, Int. J. Mass. Spectrom. Ion Processes 178 (1998) 19.
[49] H. Wu, S.R. Desai, L.S. Wang, J. Chem. Phys. 103 (1995) 4363.
[50] H. Wu, S.R. Desai, L.S. Wang, J. Phys. Chem. A 101 (1997) 2103.
[51] J.C. Rienstra-Kiracofe, G.S. Tschumper, H.F. Schaefer, Chem. Rev. 102 (2002) 231.
[52] W.C. Martin, A. Musgrove, S. Kotochigova, J.E. Sansonetti, Ground Levels and Ionization Energies for the Neutral Atoms, National Institute of Science and Technology (USA), available from: <http://physics.nist.gov/IonEnergy>.
[53] A. Daoudi, A.T. Benjelloun, J.P. Flament, G. Berthier, J. Mol. Spectrosc. 194 (1999) 8.
[54] F. Misaizu, M. Furuhashi, Y. Yamakita, K. Ohno, Eur. Phys. J. D 9 (1999) 301.
[55] A. Luna, M. Alcami, O. Mó, M. Yáñez, Chem. Phys. Lett. 320 (2000) 129.
[56] R.B. Metz, C. Nicolas, M. Ahmed, S.R. Leone, J. Chem. Phys. 123 (2005) 114313.
[57] T. Baruah, R.R. Zope, M.R. Pederson, Phys. Rev. A 69 (2004) 023201.
[58] D. Hippe, S.D. Peyerimhoff, Mol. Phys. 76 (1992) 293.
[59] A. Delabie, K. Pierloot, J. Phys. Chem. A 106 (2002) 5679.
[60] Y.R. Luo, Comprehensive Handbook of Chemical Bond Energies, CRC Press, Boca Raton, FL, 2007.
[61] M.L. Polak, M.K. Gilles, J. Ho, W.C. Lineberger, J. Phys. Chem. 95 (1991) 3460.
[62] NIST Standard Reference Database Number 69, available from: <http://webbook.nist.gov/chemistry/>.
[63] K.P. Huber, G. Herzberg, Molecular Spectra and Molecular Structure IV. Constants of Diatomic Molecules, Van Nostrand, New York, 1979.
[64] S. Smoes, F. Mandy, A. van der Auwera-Mahieu, J. Drowart, Bull. Soc. Chim. Belg. 81 (1972) 45.
[65] S. Midda, N.C. Bera, I. Bhattacharyya, A.K. Das, J. Mol. Struct. (Theochem) 725 (2005) 251.
[66] S. Midda, N.C. Bera, I. Bhattacharyya, A.K. Das, J. Mol. Struct. (Theochem) 761 (2006) 17.
[67] S. Krückeberg, L. Schweikhard, J. Ziegler, J. Chem. Phys. 114 (2001) 2955.
[68] K. Jug, B. Zimmermann, P. Calaminici, A.M. Köster, J. Chem. Phys. 116 (2002) 4497.
[69] G.L. Gutsev, C.W. Bauschlicher, J. Phys. Chem. A 107 (2003) 4755.

[70] O. Ingólfsson, U. Busolt, K. Sugiwara, J. Chem. Phys. 112 (2000) 4614.
[71] L. Mahé, S. Boughdiri, J.C. Barthelat, J. Phys. Chem. A 101 (1997) 4224.
[72] B. Dai, L. Tian, J. Yang, J. Chem. Phys. 120 (2004) 2746.
[73] S. Boughdiri, B. Tangour, M. Dachraoui, J. Chim. Phys. 90 (1993) 2039.
[74] C.W. Bauschlicher, S.R. Langhoff, H. Partridge, M. Sodupe, J. Phys. Chem. 97 (1993) 856.
[75] S.G. Wang, W.H.E. Schwarz, J. Chem. Phys. 109 (1998) 7252.
[76] R.D. Levin, S.G. Lias, Ionization Potential and Appearance Potential Measurements 1971–1981, NSRDS-NBS71, National Bureau of Standards (USA), Washington, DC, 1982.
[77] X.B. Wang, L.S. Wang, W.R. Wiley, R. Brown, P. Schwerdtfeger, D. Schröder, H. Schwarz, J. Chem. Phys. 114 (2001) 7388.
[78] K.E. Nizzi, C.A. Pommerening, L.S. Sunderlin, J. Phys. Chem. A 102 (1998) 7674.